Uncertainty in Soil Moisture Retrievals Using the SMAP Combined Active–Passive Algorithm for Growing Sweet Corn

Pang-Wei Liu, *Member, IEEE*, Jasmeet Judge, *Senior Member, IEEE*, Roger D. De Roo, *Member, IEEE*, Anthony W. England, *Fellow, IEEE*, and Tara Bongiovanni

***Abstract*—The baseline active and passive (AP) algorithm of the NASA Soil Moisture Active Passive (SMAP) mission disaggregates the brightness temperature (T_B) from a spatial resolution of 36 km to 9 km for the soil moisture (SM) using the radar backscattering coefficient (σ^0) at 3 km. This algorithm was derived based upon an assumption of a linear relationship between T_B and σ^0. In this study, we investigated the robustness of this assumption with plot-scale AP measurements obtained under different conditions of surface roughness and stages of growing sweet corn. The uncertainties in the estimated T_B at 9 km and, hence, the retrieved SM, due to uncertainties in the algorithm parameters, β and Γ, were assessed under different landcover heterogeneities. Overall, the linear regression was robust, with $r^2 > 0.75$ under bare soil conditions when surface scattering is dominant and >0.52 during the growing season. The uncertainties in β and Γ due to AP observations result in uncertainties in retrieved SM < 0.04 m^3/m^3 for most conditions of heterogeneity. The differences in T_B at 9 km, obtained when using β derived from vegetation water content (VWC) and using those from radar vegetation index, were also assessed. The errors in retrieved SM could reach as high as 0.5 m^3/m^3 for the worst-case scenario, when an intermediate scale contains high VWC, but the coarse scale region has low averaged VWC. These results suggest that determination of growth stages using a biophysical parameter is essential for β estimations, particularly for highly heterogeneous landcovers.**

***Index Terms*—Active and passive (AP) microwave remote sensing, NASA Soil Moisture Active Passive (NASA SMAP), radar vegetation index (RVI), soil moisture (SM), vegetation water content (VWC).**

I. Introduction

SOIL moisture (SM) is one of the dominant factors of soil heat and water transport governing meteorological, hydrological, and agricultural processes. Accurate estimates of SM are essential for improved predictions of climate, surface runoff, crop growth and yield, etc. [1]. Remotely sensed observations at microwave frequencies (0.3–300 GHz) have been widely used for SM applications, because they are highly sensitive to the dielectric changes between wet and dry soils [2]. Satellite-based microwave systems using active and/or passive techniques have provided global observations of radar backscatter (σ^0) and brightness temperature (T_B), respectively, for SM monitoring. Both active and passive (AP) microwave observations are sensitive to the SM in the near surface [3], but σ^0 is also highly sensitive to surface roughness and vegetation in addition to SM, compared to T_B [4]. For example, σ^0 at C-band (frequencies of 4–8 GHz) from the European Space Agency (ESA) Advanced SCATterometer [5], [6], ESA ENVISAT advanced synthetic aperture radar (SAR) [7], and T_B from the Japan Aerospace EXploration Agency (JAXA) Advanced Microwave Scanning Radiometer-Earth Observing System (AMSR-E) [8] and its follow-on mission, AMSR-2 [9], have been used for global SM estimations.

The observations at L-band (1–2 GHz) may be optimal for SM studies due to low attenuation in the atmosphere and better penetration through vegetation [10], particularly for SM estimations in agricultural regions [11]. The Soil Moisture and Ocean Salinity mission by ESA [12], [13] provides SM products using dual-pol T_B at a frequency of 1.41 GHz with a spatial resolution of 25–50 km and a repeat coverage of two to three days. However, passive observations are available at low spatial resolutions, at the 10 s of kilometers, which may be too coarse for applications in regional hydrology and agriculture [14], [15]. Active observations using SAR technique, such as JAXA Advanced Land Observing Satellite-2 [16] and the upcoming National Aeronautics and Space Administration (NASA) and Indian Space Research Organization SAR (NISAR) mission [17], are able to provide quad-polarized (quad-pol) σ^0 at L-band with higher spatial resolutions of $<$0.1 km, every 12–14 days, that may be too infrequent for SM studies. The recently launched NASA Soil Moisture Active Passive (SMAP) mission [4] included active quad-pol observations at a frequency of 1.26 GHz with spatial resolution of 3 km and passive dual-pol observations at 1.41 GHz with spatial resolution of 36 km every two to three days. Synergistic integrations of these AP observations are able to provide SM products at an intermediate scale of 9 km [18]–[22]. The current SMAP baseline algorithm disaggregates T_B observations from coarse (C) at 36 km to intermediate scale (M) at 9 km using aggregated active observations of fine scale (F) σ^0 at 3 km to obtain the Level 2 SM product [18], [23]. Although the active observations in the SMAP are no longer available

Manuscript received June 15, 2015; revised April 12, 2016; accepted April 21, 2016. Date of publication June 13, 2016; date of current version August 12, 2016. This work and MicroWEX was supported by the NASA-Terrestrial Hydrology Program-NNX09AK29G. *(Corresponding author: Pang-Wei Liu.)*

P.-W Liu, J. Judge, and T. Bongiovanni are with the Center for Remote Sensing, Department of Agricultural and Biological Engineering, Institute of Food and Agricultural Sciences, University of Florida, Gainesville, FL 32611 USA (e-mail: bonwei@ufl.edu; jasmeet@ufl.edu; tarabongio@gmail.com).

R. D. De Roo is with the Department of Climate and Space Sciences and Engineering, University of Michigan, Ann Arbor, MI 48109 USA (e-mail: deroo@umich.edu).

A. W. England is with the Department of Electrical Engineering and Computer Science, University of Michigan, Ann Arbor, MI 48109 USA, and also with the College of Engineering and Computer Science, University of Michigan-Dearborn, Dearborn, MI 48128 USA (e-mail: england@umich.edu).

Color versions of one or more of the figures in this paper are available online at http://ieeexplore.ieee.org.

Digital Object Identifier 10.1109/JSTARS.2016.2562660

since July in 2015 due to an anomaly in the radar's power amplifier, the algorithm is still valid when using alternative active observations such as from the upcoming NISAR mission.

The combined AP algorithm is given as [18]

$$T_{B_p}(M) = T_{B_p}(C) + \beta(C)\{[\sigma^0_{pp}(M) - \sigma^0_{pp}(C)] + \Gamma[\sigma^0_{qp}(C) - \sigma^0_{qp}(M)]\} \quad (1)$$

where p and q represent V- or H- polarizations, β, in K·dB^{-1}, is the slope of the AP observations from their assumed linear relationship, and Γ is a heterogeneity correction parameter defined as $\partial\sigma_{pp}/\partial\sigma_{pq}$. The parameter Γ varies with vegetation type and polarization, but is relatively consistent under different growing stages of the same type of vegetation [18], [24], while the parameter β significantly varies with polarization, surface roughness, vegetation type, growth stage, and density. Because these parameters impact retrieved SM, the accuracy of these is essential to obtain accurate estimates of SM. A few studies have tested and evaluated the algorithm over various landcovers using airborne AP observations through synthetic studies in which the observations were aggregated to match the scales for SMAP [18], [23]–[25]. In these studies, the β values were estimated through linear regressions under different vegetation densities based upon radar vegetation index (RVI). A gap still remains in an assessment of β and Γ using accurate vegetation parameters, such as vegetation water content (VWC), and their uncertainties as propagated through the algorithm to obtain $T_{\mathrm{B}}(M)$, and, hence retrieved SM. Sources of uncertainties may include AP observations and vegetation parameters used to determine the effective range of vegetation stages for estimating β. In addition, the RVI measurements used to determine the vegetation growth stages in the current studies are affected by observation noise [26], which may introduce additional errors in β.

The goal of this study is to understand the potential impacts of uncertainties in β and Γ on estimates of $T_{\mathrm{B}}(M)$ and, hence, SM, using the combined AP algorithm for SMAP [18]. Concurrent, ground-based AP observations at high temporal resolution for bare soil and two growing seasons of sweet corn were used to estimate β and Γ. Weekly VWC measurements were conducted to monitor the change of vegetation under different growth stages and were used to determine stages of the AP observations based upon biophysical characteristics. Even though β in the current algorithm is obtained at coarse scale, the assumption of a linear relationship between T_{B} and σ^0 would hold true at finer scales as well [24], and the field-scale observations in this study provide conditions that minimize the errors due to heterogeneity within the footprint. The objectives of this study are to

1) evaluate the impacts of surface roughness and different growth stages of sweet corn on β and Γ;
2) evaluate the errors from using RVI as a surrogate for VWC in determining β during growing sweet corn;
3) quantify the uncertainties propagated from uncertainties in β and Γ and the difference due to the β values derived from VWC and RVI in estimated T_{B}(M) and retrieved SM under different levels of heterogeneities.

The results of this study will provide the lowest bounds for errors in retrieved SM from SMAP due to parameters uncertainties and also contributes robust β and Γ values for growing sweet corn to the SMAP database.

II. Experimental Observations

The Microwave, Water, and Energy Balance Experiments (MicroWEXs) are a series of season-long experiments conducted at Plant Science Research and Education Unit, operated by University of Florida (UF), in north central Florida, to monitor the microwave signatures of soil and vegetation during different stages of growth (e.g., [27]–[29]). Soil texture at the field site is sandy, a dominant soil type in the state of Florida, consisting of 89% by vol. of sand, 7.5% by vol. of clay, and 3.5% by vol. of silt. In this study, we use observations during the tenth and eleventh MicroWEXs (MicroWEX-10 and -11) in 2011 and 2012 [28], [29], respectively, which were conducted in a 65 m $\times$ 75 m field. The sensors layouts are shown in Fig. 1(a) and (b).

A. Observations Under Bare Soil Conditions

A bare soil experiment was conducted during MicroWEX-11 for 36 days, from May 9 (Day of year (DoY) 130) to June 13 (DoY 165), 2012, prior to planting corn. During the experiment, concurrent AP observations were conducted every 15 min at an incidence angle of 40°, using the UF L-band Automated Radar System (UF-LARS) [30], the UF L-band Microwave Radiometer (UF-LMR), and the Truck Mounted Radiometer System from the University of Michigan (UM-TMRS).

The UF-LARS is a network-analyzer-based radar scatterometer system providing magnitude and phase of the power ratio measurements at four polarization combinations, VV, HH, HV, and VH polarizations, with a center frequency of 1.25 GHz (λ = 24.0 cm). Table I lists specifications of the UF-LARS. A single-target calibration technique [31] using a trihedral corner-reflector was applied weekly to obtain quad-pol σ^0 from the received signal. In order to reduce the fading in radar measurements, observations of σ^0 were averaged over measurements obtained spatially along three azimuthal scans at $-9°$, 0°, and +9° with respect to due South (see Fig. 1), and nine frequency measurements at 30 MHz increments from 1130 to 1370 MHz at each azimuth angle. These observations met both spatial and spectral independence criteria given in [32]. In all, 27 samples were averaged for a backscattering measurement and the standard deviation of fading was decreased from 5.57 to 0.85 dB [33]. The overall uncertainty of radar measurements was found to be 1.71 dB from errors in angle and range measurements and radar stability during calibration [30], [34]. During the experiment, the UF-LARS was mounted on a Genie manlift set at a height of 16.2 m and an incidence angle of 40°, resulting in an observation footprint of about 9.8 m $\times$ 8.7 m.

The UF-LMR was designed and built by the Microwave Geophysics Group at the University of Michigan (UM-MGG) to observe the H-pol thermal electromagnetic emission of soil at the frequency of 1.4 GHz (λ = 21.4 cm). Table II lists specifications of the UF-LMR. An internal calibration technique [35], using measurements from sky at an elevation angle of 50° and an internal matched load, was conducted weekly to convert the measurements from output voltage to T_{B}. The noise equivalent radiometric uncertainty of the UF-LMR is less than 0.5 K and the accuracy of brightness measurements calibrated using the internal matched load was estimated to be within 2 K [27]. During the experiment, the UF-LMR was mounted on a tower at a

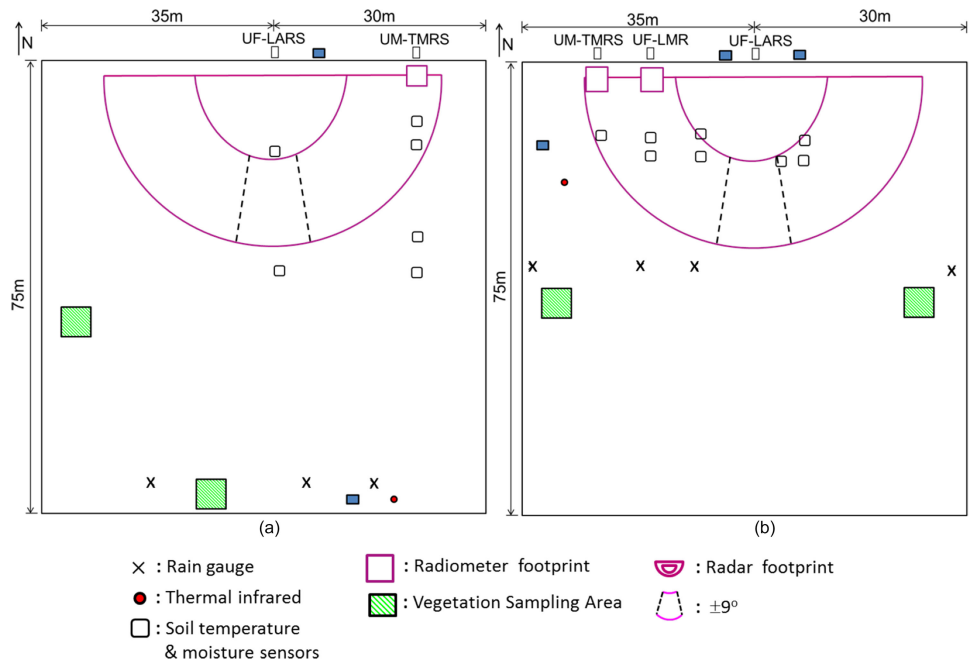

Fig. 1. Layout of sensors during (a) MicroWEX-10 and (b) MicroWEX-11. UF-LARS, UF-LMR, and UM-TMRS represent University of Florida L-band Automated Radar System, UF L-band Microwave Radiometer, and University of Michigan Truck Mounted Radiometer System, respectively. Row structure was in the east-west direction during the rough soil period and sweet corn seasons.

TABLE I
SPECIFICATIONS OF THE UF-LARS

Parameter	Qualifier	UF-LARS
Frequency(GHz)	Center	1.25
Bandwidth(GHz)		0.3
Beamwidth(degree)	3 dB (E- and H-Plane)	14.7 and 19.7
Polarization Isolation (dB)	Center/Edge	$>37/23$
Polarization		HH, VV, VH, and VH
$NE\sigma^0$ (dB)	HH/VV/VH/HV	$-23.42/-25.58/-48.12/-38.84$

TABLE II
SPECIFICATIONS OF THE UF-LMR AND UM-TMRS

Parameter	Qualifier	UF-LMR	UF-TMRS
Frequency(GHz)	Center	1.4	1.4
Bandwidth(MHz)	3 dB	20	20
Beamwidth(degree)	3 dB (E- and H-Plane)	20 and 22.5	20 and 22.5
Polarization	Sequential	H	H/V
Noise Figure (dB)	From T_{rec}	3.99	3.99

height of 8.0 m and an incidence angle of 40°, resulting in an observation footprint of about 5.6 m × 5.1 m.

Meanwhile, the UM-TMRS was installed on a boom-lift, about 6 m away from the UF-LMR, at the same height and incidence angle to observe both the V- and H-pol microwave emission at a frequency of 1.4 GHz. The UM-TMRS was built based upon the same design as UF-LMR by UM-MGG and are available for both V- and H-pol observations, as shown in Table II. During the bare soil experiment, only observations at V-pol from UM-TMRS were calibrated using the same calibration scheme as UF-LMR for this study. Table III lists the microwave sensors and amounts of data used in this study.

TABLE III
AMOUNT OF AP OBSERVATIONS DURING MICROWEX-10 AND -11 FOR THE STUDY

	UF-LARS	UF-LMR	UM-TMRS	
Experiments	Quad-pol	H-pol	H-pol	V-pol
Bare soil	2966	3268	–	2088
Sweet corn (MicroWEX-10)	3265	–	3278	3114
Sweet corn (MicroWEX-11)	3048	1459	3622	3670

In situ measurements of SM at depths of 2, 4, 8, 16, 32, and 64 cm were obtained using time-domain reflectometry (TDR) sensors from Campbell Scientific, concurrent with microwave observations. Four rain gauges were used to record the amount of water input during irrigation/precipitation events, as shown in Fig. 1(b). A linear move irrigation system was used to maintain uniform water application to the field. Fig. 1(b) shows the sensor layout during MicroWEX-11. Before the experiment, on DoY 122, the field was disked to achieve a smooth soil surface, as typically prepared prior to planting. Observations for smooth soils were used eight days later, on DoY 130, when the soil had settled down and was naturally smoothed. After 23 days, on DoY 145, a seedless planting was conducted in East–West direction [see Fig. 1(b)], using a multirow cultivators to provide a typical uniform soil roughness during the planting

TABLE IV
SOIL SURFACE ROUGHNESS MEASUREMENTS OF ROOT-MEAN-SQUARE HEIGHT (s) AND CORRELATION LENGTH (cl) USING 2-M-LONG GRID BOARD DURING BARE SOIL EXPERIMENT

DoY	Grid Board	
(2012)	s (cm)	cl (cm)
132	0.68	9.80
138	0.70	9.33
146	1.71	9.45
163	1.30	12.22

and germination stages. Soil roughness measurements, including root-mean-square height (s) and correlation length (cl), were obtained using a traditional grid board method [36], during the smooth period on DoY 132 and 138, and during the rough period on DoY 146 and 163. Six 2-D surface profiles, in direction perpendicular to the row structure, were measured using a 2-m-long grid board. The surface profile from each grid board was digitized to calculate s and l [36], individually. Each soil roughness measurement was acquired by averaging six s and l values, listed in Table IV.

Fig. 2(a)–(c) shows the concurrent AP observations and average SM at 2 cm from multiple sensors during bare soil experiment. Even though the $\sigma^0_{VH} \equiv \sigma^0_{HV}$, the noise floor of σ^0_{HV} using UF-LARS is higher than σ^0_{VH}. In this study, the σ^0_{VH} are used to represent the cross-pol observations. The VSM at 2 cm was chosen to compare the AP observations because the microwave observations at L-band are found to be sensitive to SM in 0–2 cm and the current models estimate SM within 0–2 cm [34], [37]–[39]. As shown in the figures, the variations of AP microwave observations followed the changes of SM. A sensitivity analysis of the AP observations under smooth and rough soils was conducted, as shown in Table V. During the smooth soil period, the sensitivity of active observations was estimated only when the surface scattering dominated the radar backscattering (SM $>$ 0.07 $\mathrm{m}^3/\mathrm{m}^3$). This is because the relationship between σ^0 and SM did not follow the theoretical positive linear relationship when the volume scattering was the dominant mechanism, which may complicate the sensitivity of radar observations to SM [34]. Overall, sensitivities of AP observations to SM were higher under smooth than under rough soil conditions, except the active observations at cross-pol. This is because surface roughness tends to mask the sensitivity to SM [40], but the return signals from cross-pol were too low under smooth condition, which may not be able to produce adequate strength of cross-pol observations for SM application [41]. In addition, a significant increase was observed in the radar backscatter at co- and cross-pol after the field was plowed, but the passive observations did not exhibit significant change with plowing, as they are less sensitive to changes in surface roughness [4].

B. Observations During Growing Seasons of Sweet Corn

Concurrent AP observations during two growing seasons of sweet corn were conducted during MicroWEX-10 and -11 from DoY 186 to 256 in 2011, and DoY 230 to 300 in 2012, respectively. Fig. 1(a) and (b) shows the sensor layouts during

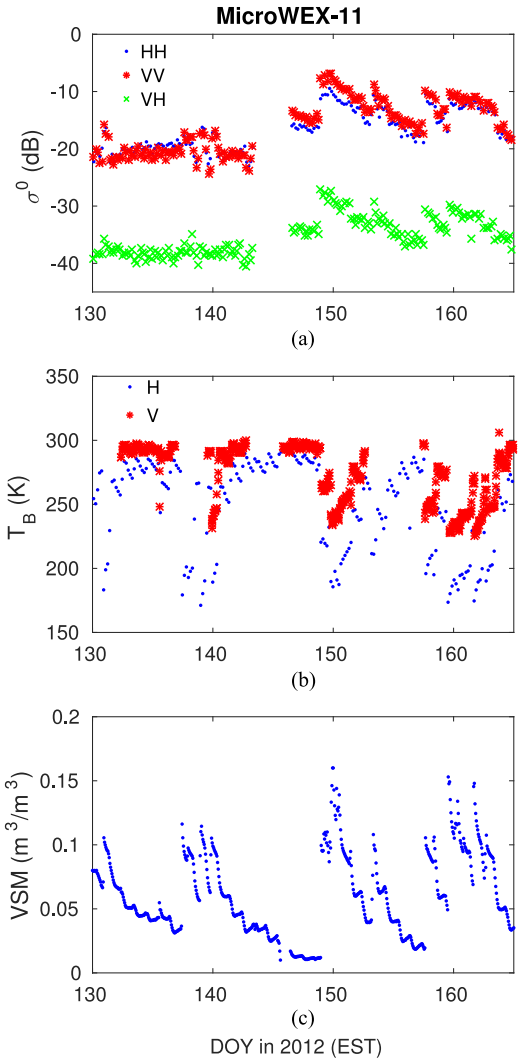

Fig. 2. Microwave observations of (a) σ^0, (b) T_B, and (c) average SM at 2 cm during bare soil experiment in MicroWEX-11. σ^0, T_BH, and T_BV were from UF-LARS, UF-LMR, and UM-TMRS, respectively.

MicroWEX-10, and -11, respectively. During MicroWEX-10, passive observations at both V- and H-pol were obtained using the UM-TMRS, while during MicroWEX-11, in addition to V- and H-pol observations from the UM-TMRS, observations of T_B at H-pol from UF-LMR were used to fill the data gaps when UM-TMRS was not available. The root-mean-square difference of T_B between the two radiometers was found to be 2.85 K, so the data inconsistency is considered to be minimal. In both growing seasons, active observations were conducted using the UF-LARS [30]. Table III lists the microwave sensors and amounts of data used in this study.

In situ SM measurements were obtained, concurrent with microwave observations, using TDRs at depths of 2, 4, 8, 16, 32, and 64 cm during both MicroWEX-10 and -11. Four rain gauges were used to record water input during the irrigation/precipitation events. Similar to the bare soil experiment, the field was disked and planted using a multirow cultivator to make the surface roughness and seed and, hence, the vegetation density uniform in the field. For both seasons, the row spacing

TABLE V
SENSITIVITY OF ACTIVE AND PASSIVE MICROWAVE OBSERVATIONS TO VSM AT 2 CM DURING BARE SOIL EXPERIMENT AND CORN GROWING SEASONS AT DIFFERENT STAGES IN MICROWEX-10 AND -11

		T_{BH}		T_{BV}		$\sigma^0_{H\,H}$		$\sigma^0_{V\,V}$		$\sigma^0_{V\,H}$	
	VWC	S_p	r^2	S_p	r^2	S_a	r^2	S_a	r^2	S_a	r^2
BS-S	–	−15.47	0.92	−9.85	0.87	2.07	0.69	2.08	0.75	0.26	0.24
BS-R	–	−8.92	0.91	−6.55	0.89	0.52	0.74	0.56	0.76	0.42	0.72
MW10-Early	0.17	−5.13	0.89	−4.57	0.82	0.32	0.54	0.44	0.72	0.45	0.78
MW10-Mid	2.50	−3.66	0.81	−3.66	0.71	0.41	0.77	0.62	0.85	0.32	0.49
MW10-Late	3.02	−2.92	0.75	−2.70	0.39	0.23	0.72	0.51	0.44	0.33	0.32
MW11-Early	0.54	−5.54	0.92	−2.80	0.85	0.39	0.69	0.34	0.79	0.50	0.76
MW11-Mid	1.13	−4.43	0.95	−1.99	0.75	0.56	0.92	0.61	0.92	0.51	0.93
MW11-Late	1.65	−4.27	0.82	–	–	0.39	0.69	0.43	0.84	0.58	0.82

The S_p and S_a represent sensitivity of radiometric and radar observations with units in $\mathrm{K}/0.01\ \mathrm{m}^3/\mathrm{m}^3$ and $\mathrm{dB}/0.01\ \mathrm{m}^3/\mathrm{m}^3$, respectively.

was 91 cm, with approximately six plants per meter. In addition, the linear move system was used for irrigation in the field to maintain the uniformity in water application. Weekly destructive vegetation samplings were conducted including measurements of leaf area index, biomass, and VWC over the seasons [28], [29].

Fig. 3(a)–(f) shows the concurrent AP observations and average SM observed at 2 cm from multiple sensors, and Fig. 4 shows the sampled VWC over the two growing seasons. A logistic regression was used to represent VWC over the growing seasons during MicroWEX-10 and -11 with r^2 of 0.95 and 0.93, respectively. During MicroWEX-10, the VWC was significantly higher after tasseling on day after planting (DAP) 38, because of higher water input and sun illumination in the Summer than during MicroWEX-11.

The growing season of sweet corn was divided into early- (before tasseling, DAP 0-38), mid- (tasseling to silking, DAP 38-50), and late-seasons (after silking, DAP 50-70), and sensitivity analyses of AP observations to SM were conducted at the three stages, during MicroWEX-10 and -11, as shown in Table V. Four-day drydown observations were used at each stage for the sensitivity estimation to ensure a wide range of SM, 0.05-0.30 $\mathrm{m}^3/\mathrm{m}^3$, and to minimize the effect due to VWC increasing over time. For the passive observations, the sensitivity decreases along with the growing seasons, because the vegetation attenuates the emission from soil [40]. For the active observations, the sensitivity increases in the mid-season, and then decreases in the late-season. This is because during the mid-season, in addition to backscattering contribution from soil, the contribution from the interaction between soil to vegetation may enhance the sensitivity of the observation, but during the late-season, the direct contribution from soil was mostly attenuated, while the interaction of soil with vegetation dominated the scattering mechanism. However, the change of dominant scattering mechanisms during growing season over time complicates the sensitivity of active observations to SM.

III. METHODOLOGY

A. β and Γ in the SMAP Combined AP Algorithm

Combinations of AP observations at V-pol, $\sigma^0_{V\,V}$-T_{BV}, and at H-pol, $\sigma^0_{H\,H}$-T_{BH}, were used to estimate β and Γ. For bare soil, β was calculated from observed T_{B} and σ^0 under different roughness conditions during MicroWEX-11, for three periods:

1) before planting, representing smooth soil ($ks \simeq 0.18$, where $k = 2\pi/\lambda$);
2) immediately after planting DoY 146 to DoY 157 (ks declining from 0.45 to 0.40), representing a typical agricultural field with high roughness;
3) under a moderate roughness condition from DoY 157 to 165 (ks declining from 0.40 to 0.35).

During the growing season, the β values were calculated from combining MicroWEX-10 and -11 AP observations based upon VWC. The effective range of VWC used to combine AP observations that provide the optimal β value was identified based upon the local maximum of r^2. Due to different mechanisms affecting microwave scattering and emission at V- and H-pols, the ranges of VWC for obtaining the β values were different for each polarization combination. The r^2 and standard error using Student's t distribution of the parameters with 95% confidence interval were used to evaluate the regression performance.

Based upon active observations during MicroWEX-10 and -11, σ^0_{pp} and $\sigma^0_{V\,H}$ are linearly related during bare soil experiment and growing sweet corn, with $r^2 > 0.8$. The parameter Γ was estimated as the slope of σ^0_{pp} to $\sigma^0_{V\,H}$ through linear regression. These β and Γ values estimated from field observations, henceforth β_{opt} and Γ_{opt}, contain minimal heterogeneity of field, therefore have minimal uncertainties, and may be considered as optimal parameters.

B. VWC Estimation Using RVI

The use of RVI as an indicator of VWC [20], [42] was examined for determination of β values [18], [23]–[25]. The RVI values were obtained using radar observations during MicroWEX-10 and -11 and were averaged daily to minimize the effect of diurnal variations [20]. A linear regression analysis was conducted to model the relationship between the averaged RVI and observed VWC. This relationship was applied to estimate VWC, which was assumed to remain constant during a day. The RVI-derived VWC were used to estimate the β values, henceforth β_{rvi}, using the same ranges of VWC as mentioned in Section III-A. This process is similar to the typical current practice when observed VWC is not available [18], [23]–[25]. The parameters β_{rvi} and β_{opt} were compared with each other and the differences between these were propagated through the AP algorithm to errors in the estimated $T_{\mathrm{B}}(M)$, representing errors due to deriving VWC from RVI.

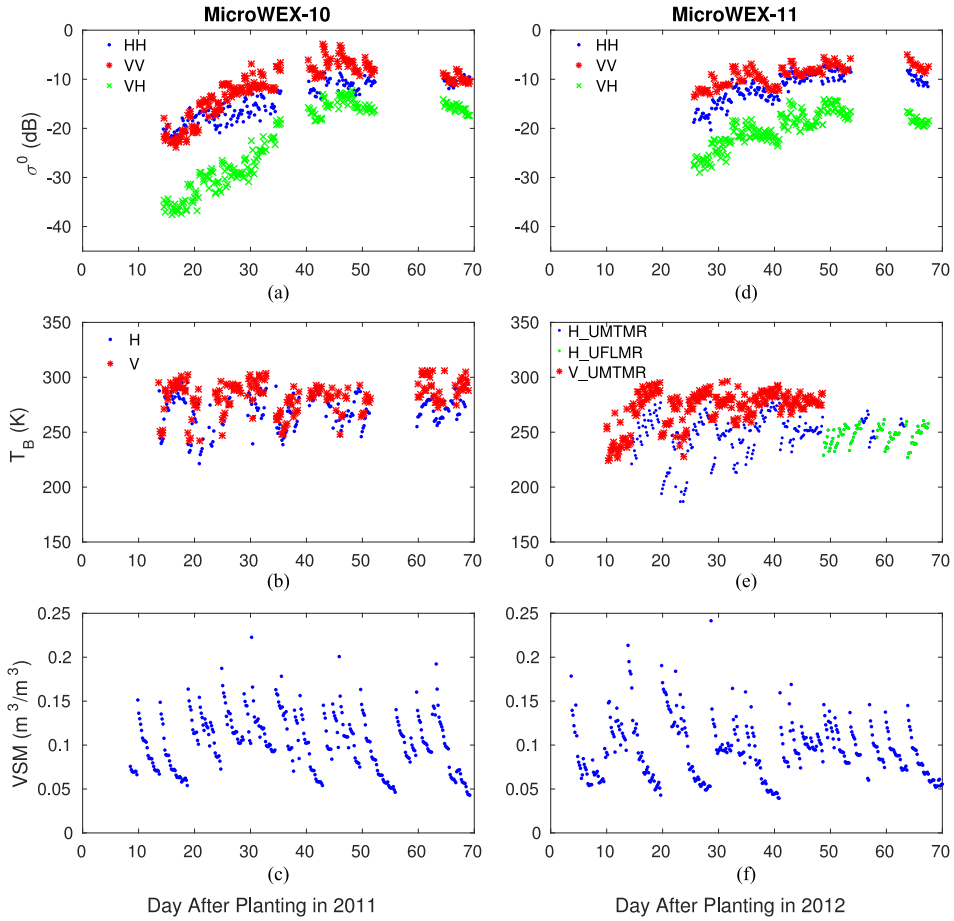

Fig. 3. Microwave observations of (a) σ^0, (b) T_{B}, and (c) average SM at 2 cm of the sweet corn during MicroWEX-10, and (d) σ^0, (e) T_{B}, and (f) average SM at 2 cm of the sweet corn during MicroWEX-11. The green dots in (c) indicate H-pol T_{B} obtained from UF-LMR to fill the data gaps during MicroWEX-11.

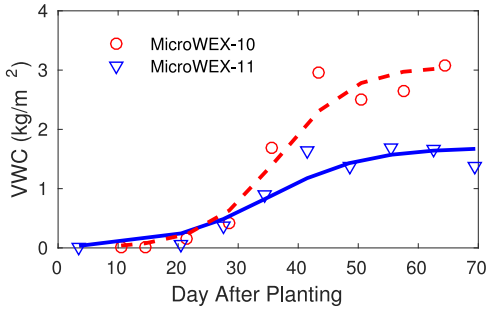

Fig. 4. VWC measurements during growing seasons in MicroWEX-10 and -11. Markers indicate measured data, while the curves are a logistic regression used to interpolate the data.

TABLE VI
COEFFICIENTS OF β AND Γ FOR VV-V AND HH-H POL DURING SMOOTH (S) AND ROUGH (R) BARE SOILS AND THEIR UNCERTAINTIES WITH 95 % CONFIDENCE INTERVAL AND r^2

	VV-V			HH-H		
	β (K·dB^{-1})	$\Delta\beta$ (K·dB^{-1})	r^2	β (K·dB^{-1})	$\Delta\beta$ (K·dB^{-1})	r^2
S:VSM $<$ 0.07	1.29	0.32	0.27	4.89	0.53	0.30
S:VSM $\geq$ 0.07	−10.76	1.10	0.83	−13.04	0.74	0.75
R:ks = 0.35-0.40	−7.99	0.25	0.86	−12.08	0.39	0.85
R:ks = 0.40-0.45	−6.21	0.28	0.81	−10.87	0.28	0.86
	Γ	$\Delta\Gamma$	r^2	Γ	$\Delta\Gamma$	r^2
R:ks = 0.35-0.45	1.04	0.03	0.85	0.90	0.02	0.80

C. Uncertainties in $T_B(M)$ Due to β and Γ

The uncertainty in the estimated T_{B} at M scale in (1) due to the uncertainties in β and Γ is given as

$$\Delta T_{B_p}(M) = \beta\Delta\Gamma[\sigma^0_{qp}(C) - \sigma^0_{qp}(M)] + \Delta\beta\{[\sigma^0_{pp}(M) - \sigma^0_{pp}(C)] + (\Gamma + \Delta\Gamma)[\sigma^0_{qp}(C) - \sigma^0_{qp}(M)]\} \quad (2)$$

where $\Delta\beta$ and $\Delta\Gamma$ are uncertainties of β and Γ, respectively. The uncertainties are estimated from standard errors of β and Γ from data regression, with 95% confidence interval using the Student's t-distribution, as mentioned in Section III-A. The values of β, $\Delta\beta$, Γ, and $\Delta\Gamma$ can be obtained from lookup tables (such as Tables VI and VII). The $\Delta T_{B_p}(M)$ will be higher for heterogeneous field, when $\sigma^0(C)$ and $\sigma^0(M)$ are significantly different. In this study, we investigate this impact in a synthetic landscape with various levels of heterogeneities. In the SMAP baseline algorithm, there are 144 F-scale pixels in every C-scale pixel and nine F-scale pixels in every M-scale pixel, as shown in

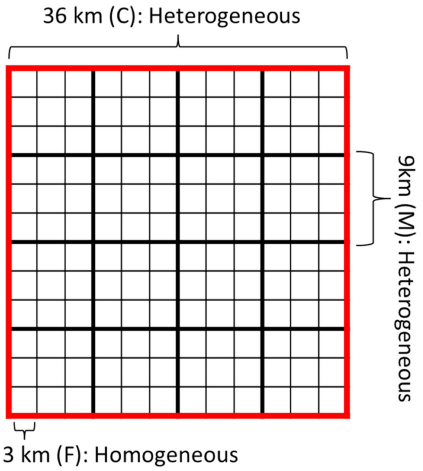

Fig. 5. Illustration of coarse (C), intermediate (M), and fine (F) scale pixels in the SMAP baseline algorithm.

Fig. 5. In this study, the C- and M-scale pixels were simulated as mixtures of bare soil and vegetated pixels at F-scale. The $\sigma^0(C)$ and $\sigma^0(M)$, in (2), were obtained through averaging the $\sigma^0(F)$ [23], [25], so the spatial distribution of the $\sigma^0(F)$ does not affect the values of $\sigma^0(C)$ and $\sigma^0(M)$.

Observations from bare soil and mature sweet corn, with VWC of 3.04 kg/m^2, were used for pixels at F-scale for the simulated scenes. This was the maximum observed VWC during the two MicroWEXs, and was used to ensure that the entire range of VWC values from very dense to sparse vegetation are accounted for. By simulating fractional vegetation from 0 to 1 in C- and M-scale pixels, the VWC range also covers values from early- to late-season to simulate VWC changes during the growing season. The $\sigma^0(F)$ under bare soil and mature sweet corn were obtained from active observations, on DOY 165, 2012, and DAP 65, 2011, respectively. The observations were averaged during a 2-h period to reduce the fading in radar observations when the SM at 2 cm was 0.09 m^3/m^3. This also ensured that the uncertainty of estimated $T_{\rm B}(M)$ in (2) is only affected by the heterogeneous distribution of sweet corn in the C-scale pixel and not by SM variations.

The VWC in the C-scale pixel can be estimated by multiplying the fraction of vegetation pixels to 3.04 kg/m^2, to obtain $\beta_{\rm opt}$ and its corresponding $\Delta\beta_{\rm opt}$, from a lookup table, as mentioned in Section III-A. The uncertainties in estimated $T_{\rm B}(M)$ due to uncertainties in β and Γ were calculated, under different levels of heterogeneity. A sensitivity analysis was conducted using the L-MEB emission model in [43] to evaluate the uncertainties in retrieved SM due to the uncertainty in estimated $T_{\rm B}(M)$.

D. Differences in $T_B(M)$ Due to $\beta_{\rm opt}$ and $\beta_{\rm rvi}$

The difference in estimated $T_{\rm B}(M)$ due to using $\beta_{\rm opt}$ and $\beta_{\rm rvi}$ is obtained as

$$\Delta T_{B_{p,\rm diff}}(M) = T_{B_{p,\rm rvi}}(M) - T_{B_{p,\rm opt}}(M) \tag{3}$$

where the $T_{\rm B_{p,rvi}}(M)$ and $T_{\rm B_{p,opt}}(M)$ represent $T_{\rm B}(M)$ from (1) by using $\beta_{\rm rvi}$ and $\beta_{\rm opt}$, respectively. Because the RVI is vulnerable to errors in the radar observations [26], using the RVI as surrogate for VWC during growing vegetation may produce incorrect β for the AP combined algorithm. This study also investigates the impact of such a difference in $T_{\rm B}(M)$ that may introduce additional errors in retrieved SM under various levels of heterogeneities, as mentioned in Section III-C. The RVI in the C-scale pixel is obtained from $\sigma^0(C)$ and to determine $\beta_{\rm rvi}$ from Section III-B, and $\beta_{\rm opt}$ is obtained as mentioned in Section III-C.

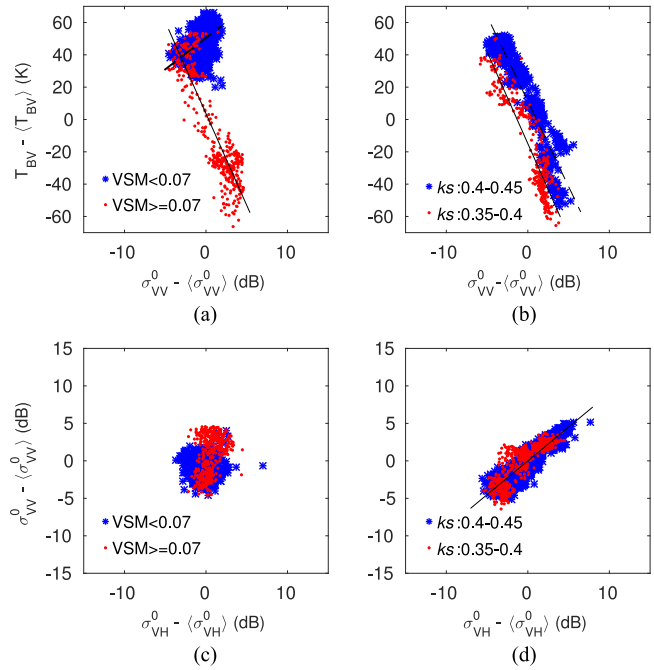

Fig. 6. Scatter plots of σ^0_{VV} and $T_{\rm BV}$ shifted by their respective means under (a) smooth and (b) rough soil conditions during MicroWEX-11, and comparisons of σ^0_{VV} and σ^0_{VH} shifted by their respective means under (c) smooth and (d) rough soil conditions during MicroWEX-11.

IV. Results and Discussion

A. β and Γ Parameters Under Bare Soil Conditions

The σ^0_{VV}-$T_{\rm BV}$ and σ^0_{HH}-$T_{\rm BH}$ perform similarly so only σ^0_{VV}-$T_{\rm BV}$ comparisons are shown here. The σ^0_{VV}-$T_{\rm BV}$ were compared under smooth and rough bare soil conditions, as shown Fig. 6(a) and (b), respectively. Under smooth and dry conditions, with ks of 0.18 and observed SM $<$ 0.07 m^3/m^3, the β value is positive and does not follow a theoretical negative trend [18], as shown in Fig. 6(a) and Table VI. This may be due to volume scattering that produces relatively high radar backscatters under smooth, dry soil [26], [34]. For SM values $>$0.07 m^3/m^3, the slope of σ^0 versus $T_{\rm B}$ is negative, as surface scattering dominates. The rough soil was separated into two periods based upon surface roughness, with ks ranges of 0.35–0.40 and 0.40–0.45, respectively, as mentioned in Section III-A. As shown in Fig. 6(b), σ^0_{VV} is inversely related to $T_{\rm BV}$ during these two periods. Unlike the smooth condition, no transition of dominant mechanisms from volume scattering to surface scattering is observed during the rough periods. A similar inverse relationship was observed between σ^0_{HH} and $T_{\rm BH}$ as well. As

TABLE VII
COEFFICIENTS OF $\beta_{\rm opt}$ AND Γ FOR VV-V AND HH-H POL DURING GROWING SEASON OF SWEET CORN AND THEIR UNCERTAINTIES WITH 95 % CONFIDENCE INTERVAL AND r^2

	VV-V				HH-H		
VWC	$\beta_{\rm opt}$ (K·dB^{-1})	$\Delta\beta$ (K·dB^{-1})	r^2	VWC	$\beta_{\rm opt}$ (K·dB^{-1})	$\Delta\beta$ (K·dB^{-1})	r^2
0.08-0.30	−7.03	0.25	0.86	0.08-0.40	−8.55	0.45	0.67
0.30-0.42	−3.67	0.32	0.71	0.40-0.60	−8.58	0.74	0.56
0.42-0.76	−6.34	0.20	0.80	0.60-1.0	−8.46	0.38	0.66
0.76-1.0	−6.60	0.43	0.64	1.0-2.0	−6.37	0.15	0.73
1.0-2.0	−3.49	0.18	0.55	2.0-3.0	−7.24	0.34	0.72
>2.0	−3.53	0.17	0.71	>3.0	−8.32	1.05	0.52
	Γ	$\Delta\Gamma$	r^2		Γ	$\Delta\Gamma$	r^2
0.08-3.25	0.59	0.01	0.84	0.08–3.25	0.55	0.01	0.85

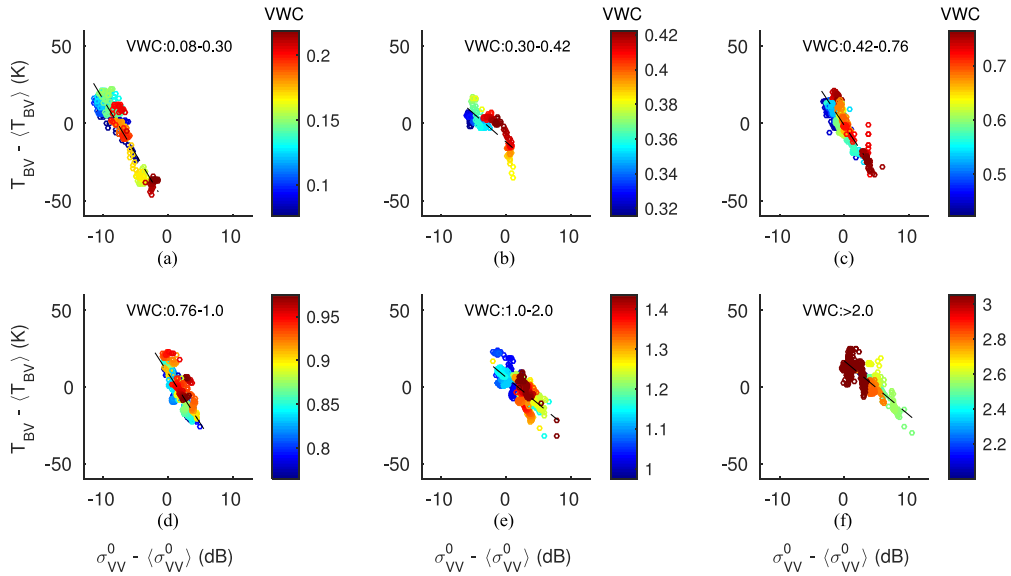

Fig. 7. Scatter plots of σ^0_{VV} and $T_{\rm BV}$ shifted by their respective means at different stages of sweet corn growth based upon VWC ranges observed during MicroWEX-10 and -11. The color bar shows VWC values during the microwave observations.

shown in Table VI, the absolute values of β, $|\beta|$, decrease as surface roughness increases, because the $T_{\rm B}$ is less sensitive to SM under rougher conditions than under smoother conditions. Even though the microwave observations are more sensitive to SM under smooth soil, the current combined AP algorithm will work only when surface scattering is dominant as it assumes an inverse linear relationship between σ^0 and $T_{\rm B}$. Similar scattering mechanisms are also observed in σ^0_{HH}–$T_{\rm BH}$, as shown in Table VI.

Observed σ^0_{VV} and σ^0_{VH} under smooth and rough soils are compared in Fig. 6(c) and (d), respectively. No significant relationship was observed under smooth soil conditions, due to low backscatter of cross-pol, approaching to the noise floor [30]. Observed σ^0_{VV} and σ^0_{VH} under rough soil conditions show a linear relationship, as in Fig. 6(d), and the Γ value was estimated using observations during two rough soil periods, as shown in Table VI. The uncertainties in Γ for both VV-V and HH-H pol are very low at 0.03 and 0.02 with r^2 of 0.85 and 0.80, respectively.

B. β and Γ Parameters During the Growing Season of Sweet Corn

Fig. 7(a)–(f) shows scatter plots of σ^0_{VV}–$T_{\rm BV}$ at different stages when their r^2 reached local maxima. Overall, all $\beta_{\rm opt}$ are at high r^2 values (0.52–0.86) and their uncertainties are $<$1.05 K·dB^{-1} with 95% confidence interval, as shown in Table VII. These results demonstrate robust linearity of AP observations at different stages of growing sweet corn based upon VWC. The r^2 values using σ^0_{VV}–$T_{\rm BV}$ are generally higher than those using σ^0_{HH}–$T_{\rm BH}$, because the σ^0_{VV} are more sensitive to SM and VWC than σ^0_{HH} [3].

Because scattering mechanisms are different at V- and H-pols, the effective regions of VWC providing the best regression results are not the same. In general, $|\beta_{{\rm opt},V}|$ values using σ^0_{VV}–$T_{\rm BV}$ decrease as VWC increases but those using σ^0_{HH}–$T_{\rm BH}$ remain very similar during the growing season. During the early season, the passive observations were more sensitive to SM than active observations, resulting in larger $|\beta_{{\rm opt},V}|$, when the AP observations are still dominated by the

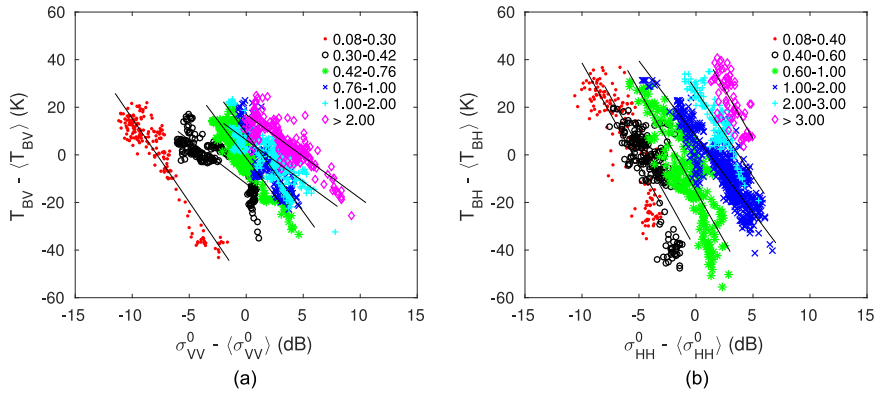

Fig. 8. Scatter plots of (a) σ^0_{VV} and $T_{\rm BV}$ and (b) σ^0_{HH} and $T_{\rm BH}$ shifted by their respective means during different stages of sweet corn growth. The markers indicate observations, and the lines indicate linear regressions as grouped by ranges of VWC ($\rm kg/m^2$) described in the legend.

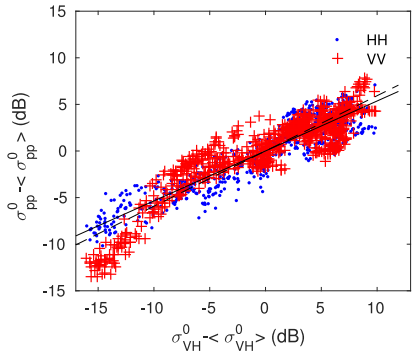

Fig. 9. Scatter plot of σ^0_{VV} and σ^0_{HH} versus σ^0_{VH} shifted by their respective means during all stages of growth of sweet corn. The markers indicate observations, and the dashed and solid lines indicate linear regressions of VV- and HH-pol data, respectively.

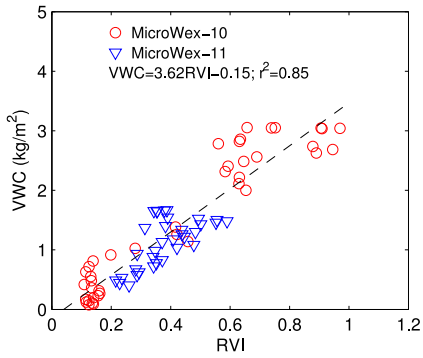

Fig. 10. Scatter plot of RVI and VWC during growing sweet corn. The markers indicate measurements and the dashed line indicates a linear regression.

contribution from soil. However, when the vegetation is fully mature during the late season, AP observations were dominated by the contribution from vegetation, and the active observations were more sensitive to vegetation than the passive observations, resulting in lower $\mid \beta_{{\rm opt},V} \mid$. Because the σ^0_{HH} are not as sensitive to vegetation as σ^0_{VV} and are close to saturation during the late season, the changes in $\mid \beta_{{\rm opt},H} \mid$ are not significant. In addition, a significant separation of σ^0_{VV}–$T_{\rm BV}$ observations was observed between stages of VWC < 0.30 $\rm kg/m^2$ and others, but no such separation was observed in σ^0_{HH}–$T_{\rm BH}$, as in Fig. 8(a) and (b). This is because σ^0_{VV} is sensitive to the vertical structure of vegetation when the height of the stem is longer than the wavelength. The significant decrease of $\mid \beta_{{\rm opt},V} \mid$ for VWC range of 0.31–0.42 $\rm kg/m^2$ may be due to the transition of the dominant backscattering contribution from the soil to the vegetation.

As shown in Fig. 9 and Table VII, the co- and cross-pol observations during the two growing seasons are approximately linear with r^2 of 0.84 and 0.85 for σ^0_{VV}–σ^0_{VH} and σ^0_{HH}–σ^0_{VH}, respectively. The uncertainties in both $\Gamma_{{\rm opt},V}$ and $\Gamma_{{\rm opt},H}$ are only 0.01 with 95% confidence interval.

C. β Parameter Using RVI-Derived VWC

Similar to the previous studies [20], [42], the r^2 and RMSE from the linear regression of RVI and VWC were 0.85 and 0.34 $\rm kg/m^2$, respectively, as shown in Fig. 10. This study discusses the difference, that could introduce additional errors, in retrieved SM at M scale due to $\beta_{\rm rvi}$ versus $\beta_{\rm opt}$ used in the combined AP algorithm. Assuming the effective ranges of growing stages for sweet corn as obtained in Section IV-B, $\beta_{\rm rvi}$ are shown in Fig. 11(a)–(f). As expected, the r^2 values during all stages are lower than $\beta_{\rm opt}$, as shown in Table VIII. Because errors in RVI-derived VWC are larger than the effective ranges of VWC, AP observations during significantly different growth stages may have been combined, resulting in higher errors in $\beta_{\rm rvi}$ compared to $\beta_{\rm opt}$. This is more apparent during early stages when the radar scattering mechanisms are still dominated by the soil, because the RVI is highly sensitive to errors in radar observation at cross-pol, particularly for lightly vegetated terrains [26].

D. Quantification of the Uncertainty in $T_B(M)$ and Retrieved SM

Uncertainties of $T_{\rm B}(M)$ were computed under different vegetation fractions within C- and M-scale pixels using (2), as mentioned in Section III-C and shown in Fig. 12(a) and (b). The values of β, $\Delta\beta$, Γ, and $\Delta\Gamma$ were obtained from Tables VI and VII for bare soil and vegetation, respectively, based upon the VWC in the C-scale pixel. When the C-scale pixel is homogeneous with a vegetation fraction of 1, implying no bare soil pixels, all M-scale pixels have vegetation fraction of 1, resulting in zero uncertainty in $T_{\rm B}(M)$ for V- and H-pol, as shown at

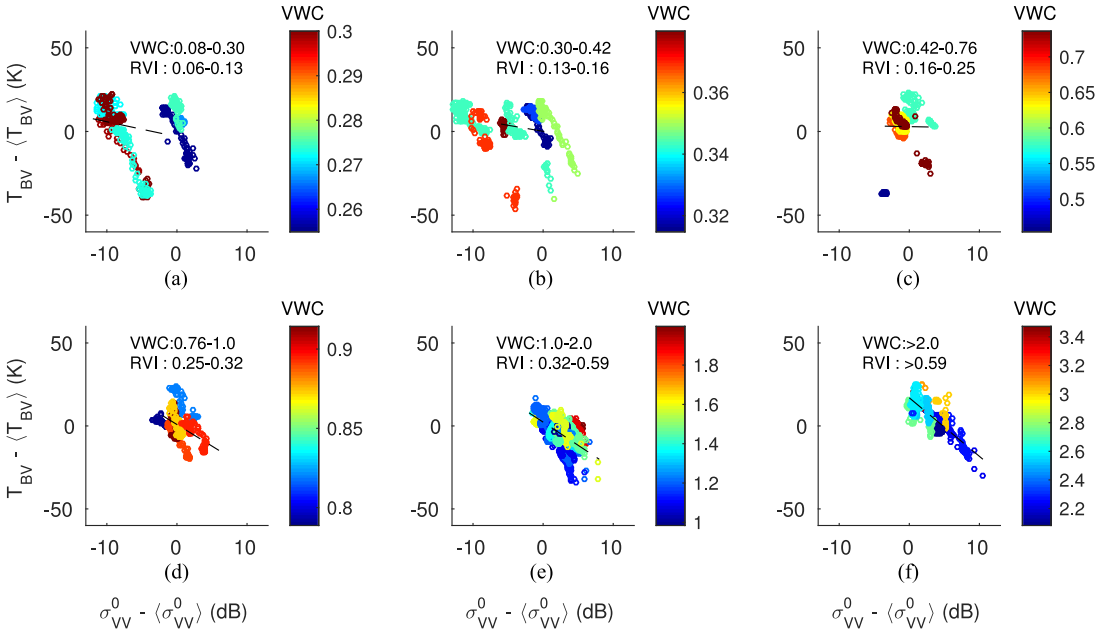

Fig. 11. Scatter plots of σ^0_{VV} and T_{BV} shifted by their respective means at different stages of sweet corn growth based upon VWC estimated from RVI during MicroWEX-10 and -11. The color bar shows estimated VWC.

TABLE VIII
COEFFICIENTS OF $\beta_{\rm rvi}$ FOR VV-V AND HH-H POL DURING GROWING SEASON OF SWEET CORN AND THEIR UNCERTAINTIES WITH 95 % CONFIDENCE INTERVAL AND r^2

	VV-V				HH-H		
VWC (kg/m^2)	$\beta_{\rm rvi}$ (K·dB^{-1})	$\Delta\beta$ (K·dB^{-1})	r^2	VWC	$\beta_{\rm rvi}$ (K·dB^{-1})	$\Delta\beta$ (K·dB^{-1})	r^2
0.08-0.30	−0.89	0.32	0.06	0.08-0.40	−4.08	0.41	0.33
0.30-0.42	−0.72	0.21	0.08	0.40-0.60	−3.53	1.76	0.08
0.42-0.76	−0.08	0.83	0.01	0.60-1.0	−1.80	0.35	0.11
0.76-1.0	−2.60	0.50	0.18	1.0-2.0	−3.26	0.27	0.20
1.0-2.0	−2.79	0.21	0.31	2.0-3.0	−4.59	0.61	0.27
>2.0	−3.53	0.19	0.70	>3.0	−4.21	0.63	0.36

the top right corner of Fig. 12(a) and (b). However, for another simulated scene, when the vegetation fraction in C-scale pixel is 0.25, there are many possible combinations of vegetation fractions (0–1) in M-scale pixels, resulting in ranges of $\Delta T_{\rm B}(M)$ from 0 to 2.4 K [see Fig. 12(a)] and 0 to 2.9 K [see Fig. 12(b)] for V- and H-pol, respectively.

Overall, uncertainties in the $T_{\rm BV}(M)$ and $T_{\rm BH}(M)$ are <2 K, except for conditions when the C-scale pixel contains significantly different VWC from that in the M-scale pixel. Typically, when the vegetation fraction in the C-scale pixel is <0.35 (VWC < 1 kg/m^2), but the vegetation fraction in the M-scale pixel is >0.8 (VWC > 2.43 kg/m^2), the uncertainties in $T_{\rm BV}(M)$ and $T_{\rm BH}(M)$ could reach as high as 2.8 and 4.9 K, respectively. These result in uncertainties in retrieved SM using V- and H-pol by as much as 0.05 and 0.06 m^3/m^3, respectively, as shown in Fig. 12(c) and (d). The SM uncertainties are slightly higher than the SMAP mission target, because the $T_{\rm B}$ is less sensitive to SM during high VWC conditions. This suggests that a higher error in retrieved SM may be introduced under conditions with low vegetated C-scale pixel but high vegetated M-scale pixel.

Similarly, when the vegetation fraction in the C-scale pixel >0.66 (VWC > 2 kg/m^2), but the vegetation fraction in the M-scale pixel is <0.4 (VWC < 1.2 kg/m^2), the uncertainties in $T_{\rm BV}(M)$ and $T_{\rm BH}(M)$ could reach as high as 1.5 and 3.2 K, respectively. These result in uncertainties in retrieved SM using V- and H-pol only 0.01 and 0.02 m^3/m^3, respectively. Overall, when applying $\beta_{\rm opt}$ and $\Gamma_{\rm opt}$ from AP observations and observed VWC in the combined AP algorithm, uncertainties in retrieved SM propagated from parameter uncertainties and heterogeneity of the field are lower than the SMAP mission target at 0.04 m^3/m^3. Even though the uncertainties in retrieved SM under a few extreme scenarios are 0.01–0.02 m^3/m^3 higher than the SMAP mission target, this will not impair the reliability of the use of field observed VWC to determine the range of growth stages for β in the agricultural regions.

E. Quantification of the Difference in $T_B(M)$ and Retrieved SM Using $\beta_{\rm opt}$ and $\beta_{\rm rvi}$

The difference in estimated $T_{\rm BV}(M)$ and $T_{\rm BH}(M)$ due to the difference in $\beta_{\rm opt}$ and $\beta_{\rm rvi}$ were computed under different

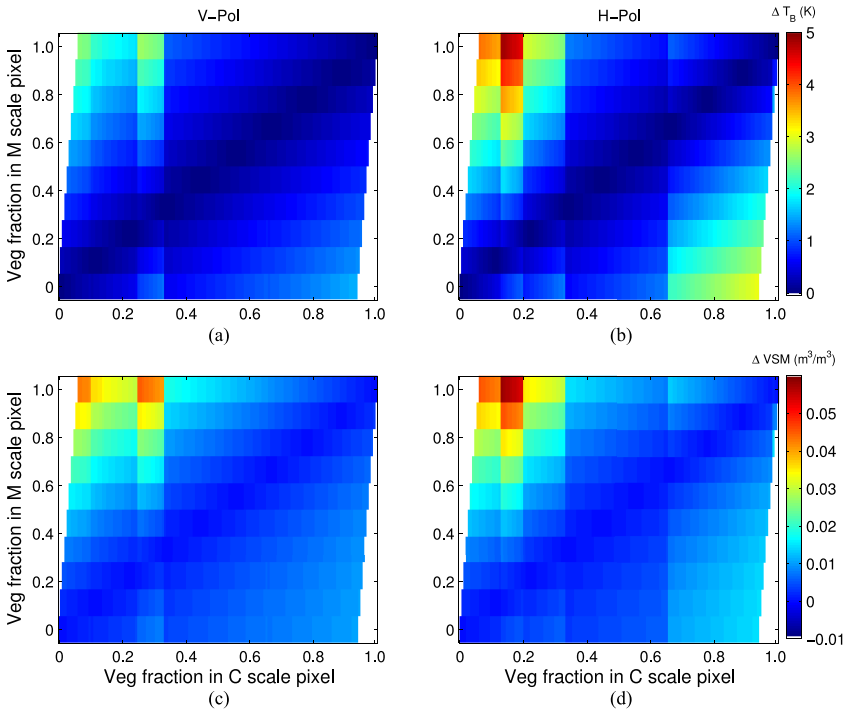

Fig. 12. Uncertainty in $T_{\mathrm{B}}(M)$ at (a) V-pol and (b) H-pol, and the uncertainty in the retrieved SM using (c) $T_{\mathrm{BV}}(M)$ and (d) $T_{\mathrm{BH}}(M)$ under different combinations of vegetation fraction in C- and M-scale pixels.

vegetation fractions within C- and M-scale pixels using (3), as mentioned in Section III-D and shown in Fig. 13(a) and (b), respectively. The β_{opt} and β_{rvi} were obtained from Tables VII and VIII using VWC and RVI in the C-scale pixels. Typically, there are two scenarios for which the combined AP algorithm is most prone to errors: first, when the M-scale pixel contains high fraction of vegetation, hence high VWC, but is embedded in a C-scale pixel with low vegetation fraction, and second, when the M-scale pixel has low vegetation fraction embedded in a C-scale pixel that has a high vegetation fraction, as shown in Section IV-D. These errors would be amplified when the difference between β_{opt} and β_{rvi} becomes significant.

For the V-pol, when the vegetation fraction in the C-scale pixel is <0.5 (VWC <1.5 kg/m^2), but the vegetation fraction in the M-scale pixel is >0.7 (VWC > 2.1 kg/m^2), the differences in the $T_{\mathrm{BV}}(M)$ can reach as much as 29.4 K. This is due to a large difference between β_{opt} and β_{rvi} when the VWC in the C-scale is relatively low, and such an impact was amplified through the AP algorithm under highly heterogeneous landcovers. Such difference in $T_{\mathrm{BV}}(M)$ result in a difference in SM by as much as 0.49 m^3/m^3, as shown in Fig. 13(c), because of the low sensitivity of T_{B} to SM under high VWC. In another scenario, when the vegetation fraction in a C-scale pixel is >0.6 (VWC > 1.8 kg/m^2), the differences in $T_{\mathrm{BV}}(M)$ are <3.5 K, because $\beta_{\mathrm{opt},V}$ and $\beta_{\mathrm{rvi},V}$ are close to each other at such a high VWC. However, even under a relatively homogeneous terrain, when vegetation fraction in a C-scale pixel is between 0.2 and 0.5 (VWC of 0.6–1.52 kg/m^2), and the vegetation fraction in the M-scale pixel is <0.2 (VWC < 0.6 kg/m^2), the difference in $T_{\mathrm{BV}}(M)$ can reach as much as 8.6 K. This will result in a difference in SM by as much as 0.06 m^3/m^3, higher than the SMAP mission target. For the H-pol, when the vegetation fraction in the C-scale pixel is <0.35 (VWC < 1.06 kg/m^2), but the vegetation fraction in the M-scale pixel is >0.8 (VWC > 2.4 kg/m^2), the difference in $T_{\mathrm{BH}}(M)$ can reach as much as 21.7 K, resulting in difference of SM by 0.3 m^3/m^3, as shown in Fig. 13(d). In contrast, when the vegetation fraction in the C-scale pixel is >0.6 (VWC > 1.84 kg/m^2), but the vegetation fraction in the M-scale pixel is <0.4 (VWC < 1.22 kg/m^2), the difference in $T_{\mathrm{BH}}(M)$ can reach as much as 10.8 K, resulting in a difference in SM by as much as 0.05 m^3/m^3, as shown in Fig. 13(d).

We further explored whether these differences in retrieved SM using $T_{\mathrm{BV}}(M)$ and $T_{\mathrm{BH}}(M)$ meet the SMAP mission target, as shown in Fig. 13(e) and (f). For the V-pol, when the vegetation fraction in the C-scale pixel >0.5 (VWC > 1.6 kg/m^2), differences of retrieved SM for all vegetation fractions in M-scale pixels are lower than the SMAP mission target when using $T_{\mathrm{BV}}(M)$. In addition, when the vegetation fraction in the C-scale pixel is <0.5, and the difference of vegetation fractions between C- and M-scale pixels is >0.18, the differences in retrieved SM are higher than the SMAP mission target. For the H-pol, over the entire range of vegetation fraction in the C-scale pixel, the difference in retrieved SM using $T_{\mathrm{BH}}(M)$ is higher than the SMAP mission target when the difference of vegetation fractions between C- and M-scale pixels is >0.23.

These results show that the difference in $T_{\mathrm{B}}(M)$, and hence, in retrieved SM, due to the difference from using β_{opt} or β_{rvi} is nonnegligible, particularly for highly heterogeneous landcovers. Therefore, quality flags may need to be applied under such conditions when accurate VWC is not available. In addition, the development of a more sophisticated algorithm that is able to accurately estimate VWC from microwave observations for β values is suggested.

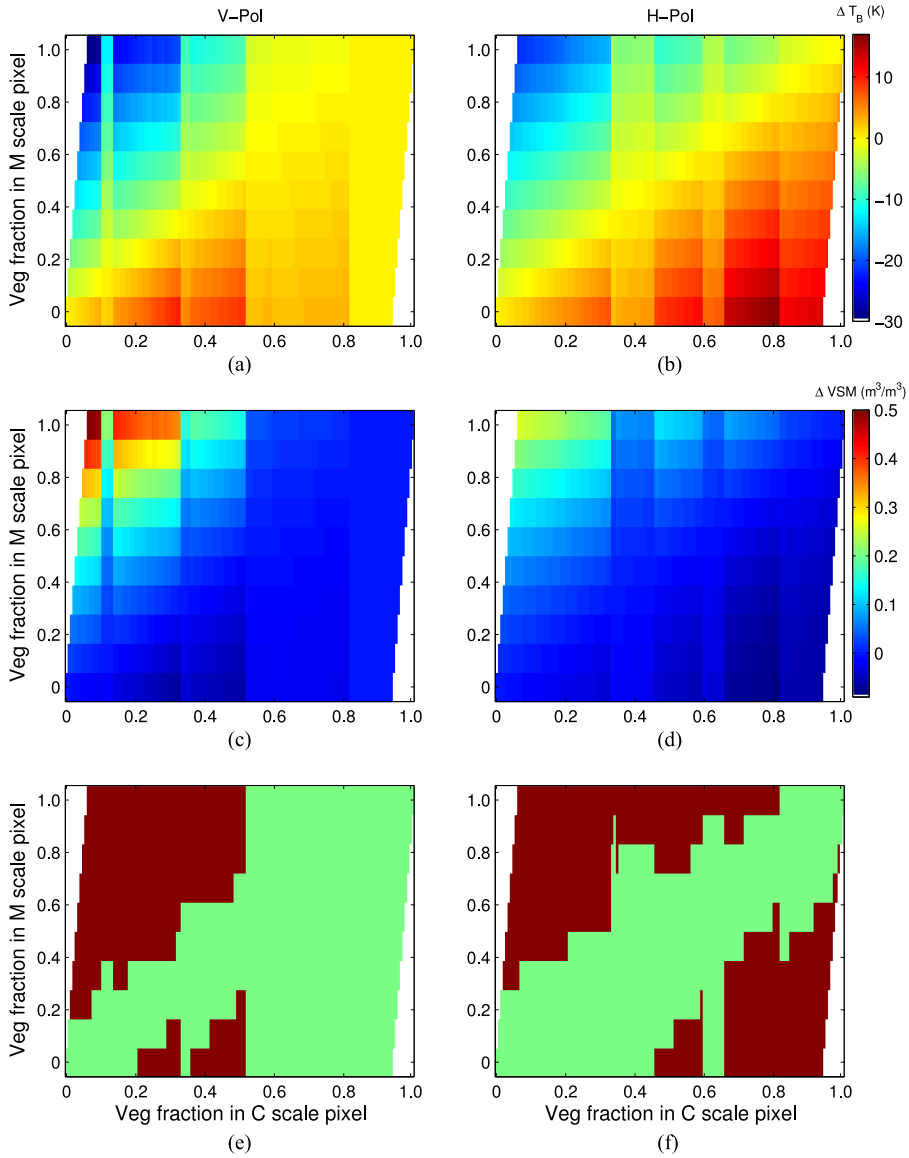

Fig. 13. Difference in $T_{\mathrm{B}}(M)$ due to the difference in β_{opt} and β_{rvi} for (a) V-pol and (b) H-pol, and the difference in the retrieved SM due to (c) $\Delta T_{\mathrm{BV}}(M)$ and (d) $\Delta T_{\mathrm{BH}}(M)$ under different combinations of vegetation fraction in C- and M-scale pixels. The conditions that the differences of retrieved SM meet the SMAP mission target of 0.04 $\mathrm{m}^3/\mathrm{m}^3$ using (e) $T_{\mathrm{BV}}(M)$ and (f) $T_{\mathrm{BH}}(M)$, where the brown and green colors show higher and lower than the target, respectively.

V. Summary and Conclusion

This study evaluates the linearity of AP observations under different surface roughness and growth stages of sweet corn and their impacts on the β and Γ for the current combined AP algorithm. During the smooth dry bare soils, AP observations did not follow a theoretical negative-sloped linear relationship. This will mislead the algorithm and result in incorrect $T_{\mathrm{B}}(M)$ estimation for SM retrieval. When the surface backscatter is the dominant scattering mechanism, AP observations exhibit robust linearity with $r^2 > 0.75$ for both V- and H-pol. During the growing season of sweet corn, linear relationship between AP observations were still true with $r^2 > 0.52$ for both V- and H-pol. For V-pol, the β values change, following the variable sensitivity of the backscatter to the vegetation growth stage, but they are relatively consistent over the growing season for H-pol. However, when using RVI as a surrogate for VWC to determine an appropriate β value for the AP algorithm, incorrect β values were produced because RVI is particularly sensitive to errors in the cross-pol observations.

The uncertainties in the $T_{\mathrm{B}}(M)$ due to β and Γ values under different levels of heterogeneities were quantified. The results show that when the vegetation fractions in the M- and C-scale pixels are significantly different by >0.6, equivalent to 1.8 kg/m^2, the propagated uncertainties in retrieved SM were as high as 0.06 $\mathrm{m}^3/\mathrm{m}^3$, a bit higher than the SMAP mission target. The difference in the $T_{\mathrm{B}}(M)$ due to the difference from using β_{opt} versus β_{rvi}, that may introduce additional errors, was also evaluated. The difference in the retrieved SM could reach as high as 0.5 $\mathrm{m}^3/\mathrm{m}^3$, when the vegetation fraction is >0.8 in the M-scale pixel but <0.2 in the C-scale pixel. This suggests that a quality flag may need to be applied for these highly heterogeneous terrains where accurate vegetation parameters are not available for the determination of growth stages.

This study used AP and vegetation observations from two season-long field experiments to explore the potential errors that may be introduced into the SMAP SM product by using the combined AP algorithm when the SMAP radiometer field of view is heterogeneous. This algorithm often works within the SMAP requirement of SM retrieval within 0.04 m^3/m^3, but in some highly heterogeneous cases the error exceeds this value. Another contribution of this paper is the tabulation of β values for sweet corn under various growth stages. A further finding is that the use of RVI to determine the appropriate growth stage introduces significant errors in the retrieved SM, and we suggest the development of a more sophisticated algorithm to determine the vegetation growth stage.

REFERENCES

[1] J. Judge, "Microwave remote sensing of soil water: Recent advances and issues," *Trans. ASABE*, vol. 50, no. 5, pp. 1645–1649, 2007.

[2] F. Ulaby, R. More, and A. Fung, *Microwave Remote Sensing: Active and Passive. Vol. III*. Boston, MA, USA: Artech House, 1986.

[3] Y. Du, F. Ulaby, and M. Dobson, "Sensitivity to soil moisture by active and passive microwave sensors," *IEEE Trans. Geosci. Remote Sens.*, vol. 38, no. 1, pp. 105–114, Jan. 2000.

[4] D. Entekhabi *et al.*, "The soil moisture active passive (SMAP) mission," *Proc. IEEE*, vol. 98, no. 5, pp. 704–716, May 2010.

[5] A. Gruber *et al.*, "Performance inter-comparison of soil moisture retrieval models for the METOP-A ASCAT instrument," in *Proc. IEEE Int. Geosci. Remote Sens. Symp.*, Jul. 2014, pp. 2455–2458.

[6] Z. Bartalis *et al.*, "Initial soil moisture retrievals from the METOP-A Advanced Scatterometer (ASCAT)," *Geophys. Res. Lett.*, vol. 34, p. L20401, 2007, doi:10.1029/2007GL031088.

[7] S. Paloscia, P. Pampaloni, S. Pettinato, and E. Snati, "A comparison of algorithms for retrieving soil moisture from ENVISAT/ASAR images," *IEEE Trans. Geosci. Remote Sens.*, vol. 46, no. 10, pp. 3274–3284, Oct. 2008.

[8] I. Mladenova *et al.*, "Remote monitoring of soil moisture using passive microwave-based techniques—Theoretical basis and overview of selected algorithms for AMSR-E," *Remote Sens. Environ.*, vol. 144, pp. 197–213, 2014.

[9] Q. Wu, H. Liu, L. Wang, and C. Deng, "Evaluation of AMSR2 soil moisture products over the contiguous united using in situ data from the international soil moisture network," *Int. J. Appl. Earth Observ. Geoinf.*, vol. 45, pp. 187–199, 2016.

[10] S. Paloscia, S. Pettinato, E. Santi, C. Notarnicola, L. Pasolli, and A. Reppucci, "Soil moisture mapping using Sentinel-1 images: Algorithm and preliminary validation," *Remote Sens. Environ.*, vol. 134, pp. 234–248, 2013.

[11] W. Crosson, A. Limaye, and C. Laymon, "Parameter sensitivity of soil moisture retrievals from airborne L-band radiometer measurements in SMEX02," *IEEE Trans. Geosci. Remote Sens.*, vol. 43, no. 7, pp. 1517–1528, Jul. 2005.

[12] Y. Kerr, *et al.*, "The SMOS mission: New tool for monitoring key elements of the global water cycle," *Proc. IEEE*, vol. 98, no. 5, pp. 666–687, May 2010.

[13] A. Bitar *et al.*, "Evaluation of SMOS soil moisture products over continental U.S. using the SCAN/SNOTEL network," *IEEE Trans. Geosci. Remote Sens.*, vol. 50, no. 5, pp. 1572–1586, May 2012.

[14] D. Mason, J. Garcia-Pintado, H. Cloke, and S. Dance, "Evidence of a topographic signal in surface soil moisture derived from ENVISAT ASAR wide swath data," *Int. J. Appl. Earth Observ. Geoinf.*, vol. 45, Part B, pp. 178–186, 2016.

[15] S. Chakrabarti, T. Bongiovanni, J. Judge, L. Zotarelli, and C. Bayer, "Assimilation of SMOS soil moisture for quantifying drought impacts on crop yield in agricultural regions," *IEEE J. Sel. Topics Appl. Earth Observ. Remote Sens.*, vol. 7, no. 9, pp. 3867–3879, Sep. 2014.

[16] A. Balenzano *et al.*, "On the use of temporal series of L- and X-band SAR data for soil moisture retrieval. Capitanata plain case study," *Eur. J. Remote Sens.*, vol. 46, pp. 721–737, 2013.

[17] P. Rosen *et al.*, "The NASA-ISRO SAR mission—An international space partnership for science and societal benefit," in *Proc. IEEE Radar Conf.*, May 2015, pp. 1610–1613.

[18] D. Entekhabi, N. Das, E. Njoku, J. Johnson, and J. Shi, "Algorithm theoretical basis document L2&L3 Radar/Radiometer Soil Moisture (Active/Passive) Data Products: Initial release, v.1," Jet Propulsion Lab., California Inst. Technol., Pasadena, CA, USA, Tech. Rep. JPL Publication JPL 400-1567, 2012. [Online]. Available: http://nsidc.org/data/smap/pdfs/atbds/l2&3_sm_ap_initrel_v11_6.pdf

[19] U. Narayan, V. Lakshmi, and T. Jackson, "High-resolution change estimation of soil moisture using L-band radiometer and radar observations made during the SMEX02 experiments," *IEEE Trans. Geosci. Remote Sens.*, vol. 44, no. 6, pp. 1545–1554, Jun. 2006.

[20] Y. Kim and J. van Zyl, "A time-series approach to estimate soil moisture using polarimetric radar data," *IEEE Trans. Geosci. Remote Sens.*, vol. 47, no. 8, pp. 2519–2527, Aug. 2009.

[21] M. Piles, D. Entekhabi, and A. Camps, "A change detection algorithm for retrieving high-resolution soil moisture from SMAP radar and radiometer observations," *IEEE Trans. Geosci. Remote Sens.*, vol. 47, no. 12, pp. 4125–4131, Dec. 2009.

[22] N. Das, D. Entekhabi, and E. Njoku, "An algorithm for merging SMAP radiometer and radar data for high-resolution soil-moisture retrieval," *IEEE Trans. Geosci. Remote Sens.*, vol. 49, no. 5, pp. 1504–1512, May 2011.

[23] N. Das, D. Entekhabi, E. Njoku, J. Shi, J. Johnson, and A. Colliander, "Tests of the SMAP combined radar and radiometer algorithm using airborne field campaign observations and simulated data," *IEEE Trans. Geosci. Remote Sens.*, vol. 52, no. 4, pp. 2018–2028, Apr. 2014.

[24] X. Wu, J. Walker, N. Das, R. Panciera, and C. Rudiger, "Evaluation of the SMAP brightness temperature downscaling algorithm using active-passive microwave observations," *Remote Sens. Environ.*, vol. 155, pp. 210–221, 2014.

[25] X. Wu, J. Walker, C. Rudiger, and R. Panciera, "Effect of land-cover type on the SMAP active/passive soil moisture downscaling algorithm performance," *IEEE Geosci. Remote Sens. Lett.*, vol. 12, no. 4, pp. 846–850, Apr. 2015.

[26] K. McColl, D. Entekhabi, and M. Piles, "Uncertainty analysis of soil moisture and vegetation indices using Aquarius scatterometer observations," *IEEE Trans. Geosci. Remote Sens.*, vol. 52, no. 7, pp. 4259–4272, Jul. 2014.

[27] T. Bongiovanni *et al.*, "Field observations during the ninth microwave, water, and energy balance experiment (MicroWEX-9): from March 24, 2010 through January 6, 2011," Center Remote Sens., Univ. Florida, Gainesville, FL, USA, Tech. Rep., 2012. [Online]. Available: http://edis.ifas.ufl.edu/pdffiles/AE/AE49400.pdf

[28] T. Bongiovanni *et al.*, "Field observations during the tenth microwave, water, and energy balance experiment (MicroWEX-10): from March 1, 2011 through January 5, 2012," Center Remote Sens., Univ. Florida, Gainesville, FL, USA, Tech. Rep., 2015. [Online]. Available: http://edis.ifas.ufl.edu/pdffiles/AE/AE51200.pdf

[29] T. Bongiovanni *et al.*, "Field observations during the eleventh microwave, water, and energy balance experiment (MicroWEX-11): from April 25, 2012 through December 6, 2012," Center Remote Sens., Univ. Florida, Gainesville, FL, USA, Tech. Rep., 2015. [Online]. Available: http://edis.ifas.ufl.edu/pdffiles/AE/AE51400.pdf

[30] K. Nagarajan *et al.*, "Automated L-band radar system for sensing soil moisture at high temporal resolution," *IEEE Geosci. Remote Sens. Lett.*, vol. 11, no. 2, pp. 504–508, Feb. 2014.

[31] K. Sarabandi and F. Ulaby, "A convenient technique for polarimetric calibration of single-antenna radar systems," *IEEE Trans. Geosci. Remote Sens.*, vol. 28, no. 6, pp. 1022–1033, Nov. 1990.

[32] F. Ulaby and M. Dobson, *Handbook of Radar Scattering Statistics for Terrain*. Norwood, MA, USA: Artech House, 1989.

[33] D. Hoekman, "Speckle ensemble statistics of logarithmically scaled data," *IEEE Trans. Geosci. Remote Sens.*, vol. 29, no. 1, pp. 180–182, Jan. 1991.

[34] P.-W. Liu, J. Judge, R. DeRoo, A. England, T. Bongiovanni, and A. Luke, "Dominant backscattering mechanisms at L-band during dynamic soil moisture conditions for sandy soils," *Remote Sens. Environ.*, vol. 178, pp. 104–112, Jun. 2016.

[35] K.-J. Tien, R. De Roo, J. Judge, and H. Pham, "Comparison of calibration techniques for ground-based C-Band radiometers," *IEEE Geosci. Remote Sens. Lett.*, vol. 4, no. 1, pp. 83–87, Jan. 2007.

[36] M. Yang, K. Calvin, J. Casanova, and J. Judge, "Measurements of soil surface roughness during the Fourth Microwave Water and Energy Balance Experiment: April 18 through June 13, 2005," Center Remote Sens., Univ. Florida, Gainesville, FL, USA, Tech. Rep., 2005. [Online]. Available: http://edis.ifas.ufl.edu/AE363

[37] W. Rondinelli *et al.*, "Different rates of soil drying after rainfall are observed by the SMOS satellite and the South Fork in situ soil moisture network," *J. Hydrometeorol.*, vol. 16, pp. 889–903, 2015.

[38] P.-W. Liu, R. DeRoo, A. England, and J. Judge, "Impact of moisture distribution within the sensing depth on L- and C-band emission in sandy soils," *IEEE J. Sel. Topics Appl. Earth Observ. Remote Sens.*, vol. 6, no. 2, pp. 887–899, Apr. 2013.

[39] M. Escorihuela, A. Chanzy, J.-P. Wigneron, and Y. Kerr, "Effective soil moisture sampling depth of L-band radiometry: A case study," *Remote Sens. Environ.*, vol. 114, pp. 995–1001, 2010.

[40] V. Lakshmi, "Remote sensing of soil moisture," *ISRN Soil Sci.*, vol. 2013, 2013, Art. no. 424178, doi:10.1155/2013/424178.

[41] H. Hirosawa, S. Komiyama, and Y. Matsuzaka, "Cross-polarized radar backscatter from moist soil," *Remote Sens. Environ.*, vol. 7, pp. 211–217, 1978.

[42] Y. Kim and J. van Zyl, "Radar vegetation index for estimating the vegetation water content of rice and soybean," *IEEE Geosci. Remote Sens. Lett.*, vol. 9, no. 4, pp. 564–568, Jul. 2012.

[43] J.-P. Wigneron *et al.*, "L-band microwave emission of the biosphere (L-MEB) model: Description and calibration against experimental data sets over crop fields," *Remote Sens. Environ.*, vol. 107, no. 4, pp. 639–655, 2007.

Pang-Wei Liu (S'09–M'13) received the Ph.D. degree in agricultural engineering (with a minor in electrical engineering) from the University of Florida, Gainesville, FL, USA, in 2013.

He is currently a Postdoctoral Research Associate with the Center for Remote Sensing, Institute of Food and Agricultural Sciences, University of Florida. His research interests include active and passive microwave remote sensing modeling for soil moisture and agricultural crops under dynamic vegetation conditions, data assimilation with crop growth models, application of LiDAR for forest biomass, and GNSS-R remote sensing for terrestrial applications.

Dr. Liu is a member of the IEEE Geoscience and Remote Sensing Society and the American Geophysical Union.

Jasmeet Judge (S'94–M'00–SM'05) received the Ph.D. degree in electrical engineering and atmospheric, oceanic, and space sciences from the University of Michigan, Ann Arbor, MI, USA, in 1999.

She is currently the Director of the Center for Remote Sensing and an Associate Professor with the Department of Agricultural and Biological Engineering, Institute of Food and Agricultural Sciences, University of Florida, Gainesville, FL, USA. Her research interests include microwave remote sensing applications to terrestrial hydrology for dynamic vegetation, modeling of energy and moisture interactions at the land surface and in the vadose zone, spatial and temporal scaling of remotely sensed observations in heterogenous landscapes, and data assimilation.

Dr. Judge is the Chair of the National Academies Standing Committee on Radio Frequencies and a member of the Frequency Allocations in Remote Sensing Technical Committee in the IEEE Geoscience and Remote Sensing Society. She also serves the American Geophysical Union as the past Chair of the Remote Sensing Technical Committee in the Hydrology Section.

Roger D. De Roo (S'88–M'96) received the B.S. in Letters and Engineering degree from Calvin College, Grand Rapids, MI, USA, in 1986, and the B.S.E., M.S.E., and Ph.D. degrees in electrical engineering from the University of Michigan, Ann Arbor, MI, USA, in 1986, 1989, and 1996, respectively.

His dissertation topic was on the modeling and measurement of bistatic scattering of electromagnetic waves from rough dielectric surfaces. From 1996 to 2000, he was employed as a Research Fellow with the Radiation Laboratory, Department of Electrical Engineering and Computer Science, University of Michigan, investigating the modeling and simulation of millimeterwave backscattering phenomenology of terrain at near grazing incidence. He is currently an Associate Research Scientist and Lecturer with the Department of Climate and Space Sciences and Engineering, University of Michigan. His current research interests include digital correlating radiometer technology development, radio frequency interference mitigation, inversion of geophysical parameters such as soil moisture, snow accumulation, and vegetation parameters from radar and radiometric signatures of terrain, and ground truth techniques for those geophysical parameters. He has supervised the fabrication of numerous dual-polarization microcontroller-based microwave radiometers.

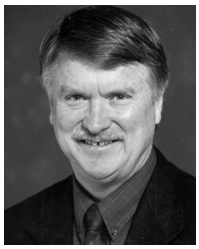

Anthony W. England (F'95) received the Ph.D. degree in geophysics from the Massachusetts Institute of Technology, Cambridge, MA, USA, in 1970.

He joined the University of Michigan, Ann Arbor, MI, USA, in 1988. He is the Dean of the College of Engineering and Computer Science, University of Michigan, Dearborn, MI, where he is a Professor of electrical and computer engineering. He is also a Professor of electrical engineering and computer science with the College of Engineering, University of Michigan, Ann Arbor. His research has spanned aspects of exploration geophysics and microwave sensing of the Earth and planets, with emphasis upon microwave radiometry of the Earths cryosphere. He participated in and led geophysical field parties in Antarctica, used radar to study glaciers in Washington and Alaska, and used microwave radiometry to develop land-surface models of permafrost on the North Slope of Alaska. He was co-Investigator on the Apollo 17 Surface Electrical Properties experiment, co-Investigator on Shuttle Imaging Radar A and C, Mission Scientist for Apollos 13 and 16, Mission Specialist astronaut on Spacelab 2, Space Station Program Scientist in 1986–1987, and Visiting Professor with Rice University in 1987–1988.

Dr. England is an Associate Editor for the *Journal of Geophysical Research*, a member of the Administrative Committee of the IEEE Geoscience and Remote Sensing Society, a member of the National Research Council's Space Studies Board, and the Chair of several federal committees concerned with science and technology. He is a Fellow of the Electromagnetics Academy and a member of the American Geophysical Union.

Tara Bongiovanni received the B.S. and M.E. degrees in agricultural and biological engineering from the University of Florida, Gainesville, FL, USA, in 2009 and 2012, respectively.

Her master's research focused on modeling crop growth and development, and on improving modeled estimates of biomass and yield through assimilating remote sensing observations. She is currently with the Center of Remote Sensing, University of Florida. Her research interests include GIS work for decision support models, which includes processing field and remotely sensed data. She also supervises crop vegetation sampling, data collection, sensor monitoring, and data archiving for the Center.